Unsteady fronts in the spin-down of a fluid-filled torus

C. del Pino,[1] R. E. Hewitt,[2] R. J. Clarke,[3] T. Mullin,[2] and J. P. Denier[4]
[1]*ETS Ingenieros Industriales, Universidad de Málaga, Pza. El Ejido s/n, Málaga 29013, Spain*
[2]*Manchester Centre for Nonlinear Dynamics, University of Manchester, Oxford Road, Manchester M13 9PL, United Kingdom*
[3]*Department of Engineering Science, University of Auckland, New Zealand*
[4]*School of Mathematical Sciences, University of Adelaide, Adelaide 5005, Australia*

(Received 31 March 2008; accepted 10 October 2008; published online 31 December 2008)

We report the results of an experimental investigation into fluid motion induced by the deceleration to rest of a rigidly rotating fluid-filled torus. Transition to a transient turbulent state is found where the onset of the complicated motion is triggered by a small-scale wavelike instability. The wave forms on a front that propagates from the inner wall of the toroidal container after it is stopped. We reveal the origins of the front through a combination of careful experimental measurements, boundary-layer analysis, and computation of the axisymmetric Navier–Stokes equations. © *2008 American Institute of Physics*. [DOI: 10.1063/1.3054146]

The fundamental mechanisms by which a (homogeneous) fluid within a rotating container adjusts to small reductions in the angular frequency are largely understood since the seminal work of Greenspan and Howard.[1] When the rotation rate of the container is changed from Ω_i to Ω_f and $|\Omega_i-\Omega_f| \ll 1$, three timescales of $O(\Omega^{-1})$, $O(\mathrm{Ek}^{-1/2}\,\Omega^{-1})$, and $O(\mathrm{Ek}^{-1}\,\Omega^{-1})$ naturally arise when the Ekman number is small. (Here $\mathrm{Ek}=\nu/\Omega_i H^2$, where ν is the kinematic viscosity and H is a typical column height of the fluid.) The first timescale is set by the development of viscous Ekman layers on bounding surfaces and the second is set by the removal of angular momentum from the fluid bulk by the slow, $O(\mathrm{Ek})$, meridional circulation induced by the Ekman layer's mass transport. Finally, residual inertial oscillations are removed on a viscous timescale. The sequence can be qualitatively similar for greater changes in rotation rate, although the introduction of nonlinear effects can lead to some novel flow phenomena. For example, during spin-up in a cylindrical container, sidewall boundary layers can become detached and propagate into the bulk flow (see Ref. 2). In this work we show evidence that unsteady separation of the boundary layer can impact the global flow response in the nonlinear regime for toroidal geometries.

When the rotating container has the form of a torus, instabilities become more evident since part of the flow field is always potentially susceptible to centrifugal instabilities. Madden and Mullin[3] considered the spin up of a fluid-filled torus from a state of rest and observed the propagation of a band of fluid from the wall into the core. This was referred to as a front (also see Fig. 2) but its origins were not definitively accounted for. In general, these fronts were found to be susceptible to nonaxisymmetric wavelike instabilities, ultimately resulting in turbulent flow. The turbulent motion was transient and eventually decayed leaving rigid-body rotation. In our present investigations we find that similar unstable fronts also exist when the torus is spun-down to rest. We make progress by complementing our measurements with an asymptotic analysis and computations of the axisymmetric Navier–Stokes equations; in this manner we are able to illuminate the mechanism that underpins the observed flow structures.

I. EXPERIMENTS

Our experimental configuration consisted of a torus filled with distilled water, which was rotated at a constant initial angular velocity Ω_i. The experiment was performed in a temperature controlled environment, and the temperature of the water in the torus was measured to be $T=19.7\pm0.3\ ^\circ\mathrm{C}$. A dc motor with feedback control connected via a gear box and belt drive was used to drive the torus. The angular velocity of the container was measured using an optical shaft encoder. In each experiment, the rotation rate was reduced from an initial value, Ω_i, to zero over 0.03 s, with minimal residual oscillation of the container.

The torus was milled in two halves from solid blocks of Perspex and bolted together. It had a radius of curvature (R) of 125 ± 0.1 mm and a cross-sectional radius (a) 16 ± 0.1 mm so that the radius ratio was $\delta=a/R=0.128$. The inner ($r^*=a$, $\theta=\pi$) and outer ($r^*=a$, $\theta=0$) equatorial regions of the torus are referred to as A and B, as in Fig. 1.

The natural nondimensional time and length variables are $t=t^*\Omega_i$ and $r=r^*/a$. A Reynolds number Re for the flow is given by

$$\mathrm{Re}=\frac{\Omega_i a R}{\nu}, \tag{1}$$

where ν is the kinematic viscosity of the fluid. Equivalently the Ekman number is $\mathrm{Ek}=1/(\delta\,\mathrm{Re})$. The tolerances of the drive mechanism and working-fluid temperature were such that the value of Re was known to be within 2%.

Flow visualization was enabled by seeding the fluid with Mearl-maid AA pearlessence and illuminating with a light sheet along the plane $\theta=0$ perpendicular to the axis of rotation. After deceleration of the torus to a state of rest, a propagating front is observed as a localized region of increased intensity in the video frames (see Figs. 2 and 3). We provide

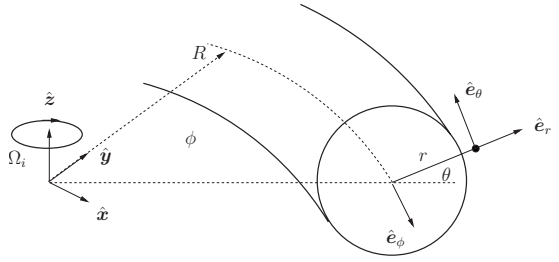

FIG. 1. Nondimensional coordinate system (r,θ,ϕ) for a torus rotating with initial angular velocity Ω_i. The coordinate system is fixed in the inertial frame.

evidence below that the observed front (at least in its early stages) is associated with the temporal development of the unsteady boundary layer at the inner equator of the container. The distance of the front from the inner equatorial wall of the torus was used as a quantitative measure of the flow response.

Precise measurements were obtained by processing successive video frames captured using a charge coupled device camera. The video contains 24 frames per second; therefore the time step between frames is 0.0417 s with a spatial resolution of between 0.08 and 0.1255 mm/pixel. The location of the front was determined from the digitized image by first extracting an intensity profile for a cross section of a single frame. An example of the grayscale intensity profile is shown in Fig. 3, across the line C-C' shown in Fig. 2.

II. THEORY

The experiments enabled us to observe the evolution of the front and provided qualitative information concerning instabilities of the flow. We now outline the development of a model, which we use to describe the initial phase of the propagation of viscous effects into the core after deceleration of the container. In particular, our focus is on events in the meridional plane of the cross section of the torus.

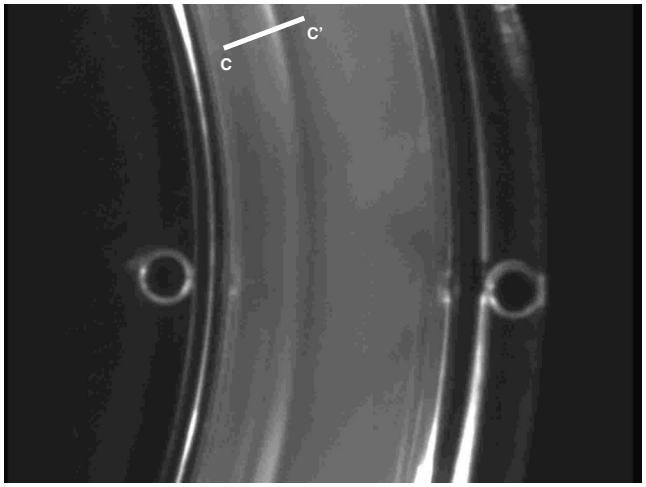

FIG. 2. Flow visualization of spin-down at $t^*=0.625$ s ($t=1.071$) after deceleration to rest with $\Omega_i=1.7136$ rad/s (Re=3420). Here we show a section of the torus with the flow viewed in the $\theta=0$ plane, which is illuminated by a thin light sheet. A front can be observed as the change in intensity of reflected light displaced from the inner equator.

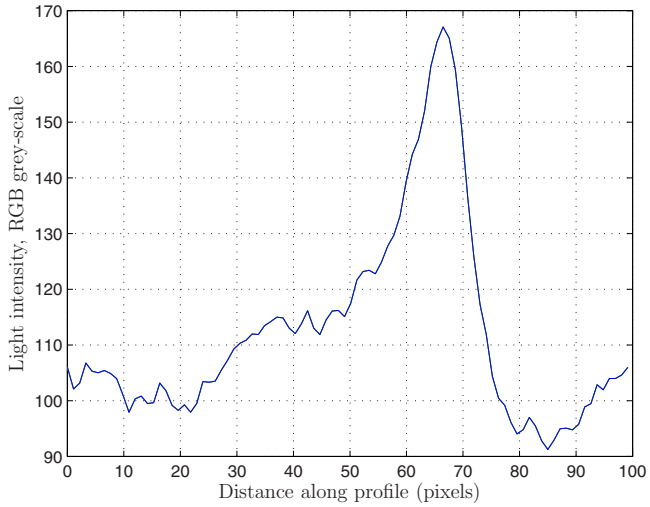

FIG. 3. (Color online) Values of the digitized (grayscale) light intensity over the line C-C' (as shown in Fig. 2 at the same parameter values). One pixel in the captured image corresponds to 0.1255 mm.

When the Reynolds number is large ($\mathrm{Ek}\ll 1$) and there is an abrupt change in the rotation rate of the torus, we expect that the initial readjustment will be mediated by a boundary layer on the wall. Clearly we could consider the entire boundary layer; however, for our purposes here it is sufficient to note that a local description is possible that is valid at the equatorial regions A and B. This local description is possible because these equatorial regions are stagnation points of the flow in the meridional plane.

The local boundary-layer description can be given in terms of the scaled coordinate $\eta>0$ defined by

$$r = 1 - \mathrm{Ek}^{1/2}\,\eta. \tag{2}$$

This approach is equivalent to the well-known unsteady (local) solution valid at the equator of an impulsively spun sphere in an otherwise quiescent fluid.[4] Near the equatorial points, where $\theta=\alpha+\vartheta$, with $|\vartheta|\ll 1$ and $\alpha=0,\pi$, we seek a local solution in the form

$$u = \mathrm{Ek}^{1/2}\,\tilde{u}(\eta,t) + \cdots, \tag{3a}$$

$$v = \vartheta\tilde{v}(\eta,t) + \cdots, \tag{3b}$$

$$w = \tilde{w}(\eta,t) + \cdots, \tag{3c}$$

$$p = \vartheta^2\tilde{P}_B + \mathrm{Ek}^{1/2}\,\tilde{P}(\eta,t) + \cdots, \tag{3d}$$

where (u,v,w) are the (dimensionless) velocity components in the directions r,θ,ϕ, respectively, and p is the pressure. Here the velocity components have been made nondimensional using the natural scale $\Omega_i a$, and the pressure term $\tilde{P}_B$ is determined from the bulk rotation. Thus

$$\tilde{P}_B = -\frac{\varrho\cos\alpha}{2}, \tag{4}$$

where $\varrho=(1+\delta\cos\alpha)/\delta$ is a dimensionless measure of the radial location relative to the axis of rotation and clearly

$\cos\alpha = \pm 1$ at $\alpha = 0, \pi$. Given this expansion, the leading-order boundary-layer equations are

$$-\frac{\partial \tilde{u}}{\partial \eta} + \tilde{v} = 0, \tag{5a}$$

$$\frac{\partial \tilde{v}}{\partial t} - \tilde{u}\frac{\partial \tilde{v}}{\partial \eta} + \tilde{v}^2 + \frac{\cos\alpha}{\varrho}\tilde{w}^2 = \varrho\cos\alpha + \frac{\partial^2 \tilde{v}}{\partial \eta^2}, \tag{5b}$$

$$\frac{\partial \tilde{w}}{\partial t} - \tilde{u}\frac{\partial \tilde{w}}{\partial \eta} = \frac{\partial^2 \tilde{w}}{\partial \eta^2}. \tag{5c}$$

We do not give the equation for the pressure correction $\tilde{P}$; it can be determined in the standard manner *a posteriori*.

It is important to note that we are able to describe the local solution in this way without determining the boundary-layer evolution for all values of θ. We thus reduce the problem to an initial-boundary-value problem for $t > 0$ and $\eta > 0$, subject to no-slip and impermeability at the torus wall $\eta = 0$ and matching to a rigid-body rotation in the bulk flow. Therefore, we require that

$$\tilde{u}(\eta,0) = \tilde{v}(\eta,0) = 0, \quad \tilde{w}(\eta,0) = \varrho, \tag{6a}$$

$$\tilde{u}(0,t) = \tilde{v}(0,t) = \tilde{w}(0,t) = 0, \quad t > 0, \tag{6b}$$

$$\tilde{v} \to 0, \quad \tilde{w} \to \varrho, \quad t > 0 \ , \text{ as } \ \eta \to \infty. \tag{6c}$$

We eliminate the explicit appearance of ϱ in Eq. (5) through the following further rescalings:

$$\eta = \varrho^{-1/4}\xi, \quad t = \varrho^{-1/2}\tau, \tag{7a}$$

$$\tilde{u}(\eta) = -\varrho^{1/4}U(\eta), \quad \tilde{v}(\eta) = -\varrho^{1/2}V(\eta), \tag{7b}$$

$$\tilde{w}(\eta) = \varrho W(\eta), \tag{7c}$$

which transforms Eq. (5) into

$$\frac{\partial U}{\partial \xi} - V = 0, \tag{8a}$$

$$\frac{\partial V}{\partial \tau} + U\frac{\partial V}{\partial \xi} - V^2 + (1 - W^2)\cos\alpha = \frac{\partial^2 V}{\partial \xi^2}, \tag{8b}$$

$$\frac{\partial W}{\partial \tau} + U\frac{\partial W}{\partial \xi} = \frac{\partial^2 W}{\partial \xi^2}, \tag{8c}$$

subject to initial conditions

$$U(\xi,0) = V(\xi,0) = 0, \quad W(\xi,0) = 1 \tag{8d}$$

and boundary conditions

$$U(0,\tau) = V(0,\tau) = W(0,\tau) = 0, \quad \tau > 0, \tag{8e}$$

$$V \to 0, \quad W \to 1, \quad \tau > 0, \quad \text{as } \ \xi \to \infty. \tag{8f}$$

As one might expect, this transformed system is closely related to that given by (for example) Simpson and Stewartson[5] for the spin-up of fluid external to a sphere. This can be seen by comparing Eq. (7) with Eq. (1.2) in their work. The main difference here is that we have a spin-down flow, in which there is a pressure distribution associated with the initial state of rotation.

The initial-boundary-value problem (7) was solved using (second-order) central differences in ξ and (second-order) time marching from an initial condition of rigid-body rotation. Time marching the local boundary-layer equations relevant to the flow near region B (the outer equator, where $\alpha = 0$) revealed that a steady state was quickly achieved. However, the same initial-value calculation for region A ($\alpha = \pi$) exhibited an evolution to a finite-time singularity. As with the impulsively spun sphere,[4] the boundary-layer assumption is eventually invalidated, with a singular boundary-layer thickness obtained.

III. COMPUTATION

In order to follow the development of the flow beyond this point, we solve the axisymmetric Navier–Stokes equations at finite Re (with velocities nondimensionalized as in the boundary-layer analysis). An assumption of axisymmetry is in accord with experimental observations prior to the onset of a wavelike instability. We introduce a streamfunction ψ to describe flows within the cross section of the torus:[6]

$$u = h^{-1}r^{-1}\partial_\theta \Psi, \quad v = -h^{-1}\partial_r \Psi, \quad \Psi = h\psi, \tag{9}$$

where $h = 1 + \delta r\cos\theta$, which ensures conservation of mass in the numerical scheme. We formulate the problem in terms of evolution equations for the axial (ϕ) components of vorticity ω and velocity w, these being

$$\partial_t \omega + \frac{2\delta w\sin\theta\partial_r w}{h} + \frac{2\delta w\cos\theta\partial_\theta w}{hr} + \frac{1}{r}\left(\frac{\partial_r \omega\partial_\theta \Psi}{h} - \frac{\delta\cos\theta\omega\partial_\theta \Psi}{h^2} - \frac{\partial_r \Psi\partial_\theta \omega}{h} - \frac{\delta r\sin\theta\Psi_r\omega}{h^2}\right) = \mathrm{Ek}\,\mathcal{L}^2\omega \tag{10a}$$

and

$$\partial_t w + u\partial_r w + \frac{v\partial_\theta w}{r} + \frac{\delta\cos\theta uw}{h} - \frac{\delta\sin\theta vw}{h} = \mathrm{Ek}\,\mathcal{L}^2 w, \tag{10b}$$

respectively, where

$$\mathcal{L}^2 \equiv \partial_{rr}^2 + \left(\frac{1}{r} + \frac{\delta\cos\theta}{h}\right)\partial_r + \frac{1}{r^2}\partial_{\theta\theta}^2 - \frac{\delta\sin\theta\partial_\theta}{hr} - \frac{\delta^2}{h^2}.$$

Both evolution equations are time stepped using an alternating direction implicit (ADI) scheme, with spatial derivatives approximated by (second-order) central differences. Once the vorticity at a given time step has been computed, the streamfunction is determined by discretizing

$$\omega = -\mathcal{L}^2\psi \tag{10c}$$

using (second-order) central differences on the same computational mesh and then solving the resulting linear system using LU decomposition. Results are generated using a uniform 200×200 grid for spatial points and a temporal step

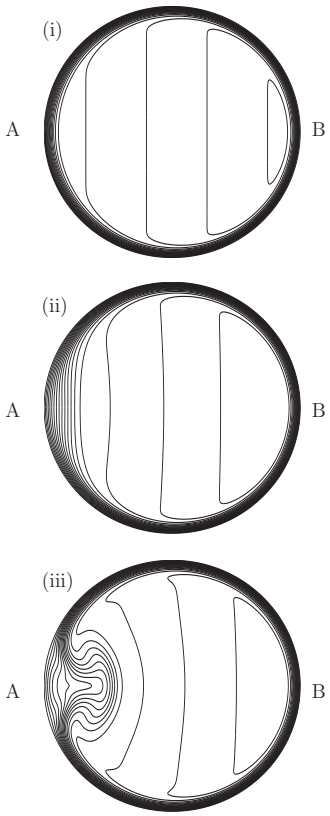

FIG. 4. Contours of the axial flow, $w(r,\theta,t)$, at times $t=0.5$, 1, 1.5 [shown as (i)–(iii), respectively] for the case Re=3420, $\delta=0.128$. Twenty uniformly spaced contour levels are shown at increments of 0.4737. The very rapid growth of the boundary-layer thickness at the inner equator (region A) is clearly shown in comparison to the quasisteady boundary layer at the outer region B.

size of 10^{-3}, with convergence verified on a 300×300 mesh and time steps of size of 2.5×10^{-4}.

In both the full Navier–Stokes simulations and the reduced boundary-layer formulations there will be difficulties at $t=0$ for an impulsive deceleration. In order to avoid this, the boundary rotation is smoothly changed to rest over a short time interval, and results were checked to be independent of the particular choice of deceleration profile.

IV. RESULTS

In Fig. 4 we show contours of the swirl velocity w at dimensionless times of $t=0.5$, 1, 1.5, as obtained by our numerical solution of the fully nonlinear axisymmetric equations at Re=3420 and $\delta=0.128$.

In Fig. 4(i) we see that the core flow is still largely in a state of rigid-body rotation as illustrated by the equally spaced contours aligned with the axis of rotation. Even at this early stage of $t=0.5$ (approximately 0.3 s after deceleration in the experimental configuration) the boundary layer is thicker near region A than B by approximately 37%.

In Fig. 4(ii) at $t=1$ (0.6 s), the effect of an increasingly rapid development of the boundary-layer thickness is seen in region A. There is also a slight drift of the core-flow contours to larger radius indicating a small degree of spin-down associated with meridional pumping of fluid through the boundary layer.

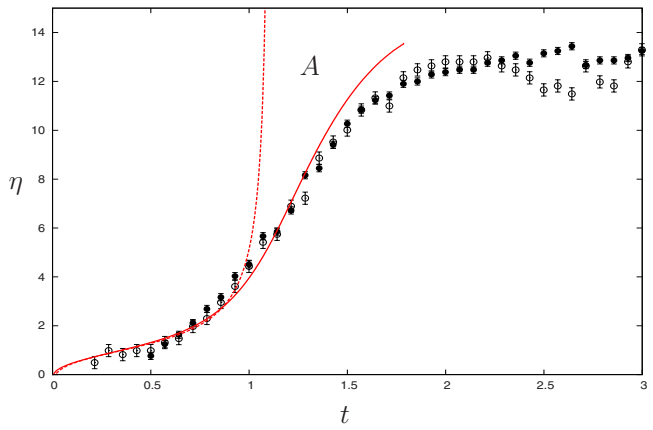

FIG. 5. (Color online) Temporal evolution of the boundary-layer thickness (Re=3420). The solid and dashed lines are the axisymmetric Navier–Stokes computations and boundary-layer (infinite-Re) predictions, respectively. Here we show two data sets (points with error bars) for the front position near region A in the torus, as measured in the laboratory experiments at two different locations around the torus. Divergence of the two data sets at later times is due to the growth of a nonaxisymmetric wave instability.

Finally, in Fig. 4(iii) at $t=1.5$ (still much less than the time 2π taken for one rotation of the container prior to deceleration) the results of an eruption of the boundary layer are seen with major disruption to the core flow. Nonetheless, we see that region B is essentially quasisteady, in agreement with the local boundary-layer model.

In Fig. 5 we present quantitative comparisons between the experimental data, boundary-layer model, and axisymmetric finite-Re results for the boundary-layer thickness (or equivalently front position) in region A. The circular markers plot the progress of the front as a function of time when Re=3420. The theoretical predictions are presented using a 75% measurement of the boundary-layer thickness, that is, the value of η at which the azimuthal component, $\tilde{w}$, is 75% of the initial (core) value. Other choices of the measure were made with no resulting qualitative change. The singular local boundary-layer result is shown as the dashed line, while the numerical finite-Re result is the solid line. Up until times $t\approx1$, good agreement is found between numerical/asymptotic predictions and the experimentally observed front position. Agreement between the axisymmetric Navier–Stokes computation and the experimental data continues until the point at which a nonaxisymmetric instability develops.

The significance of the front is that experiments show that it leads to observable small-scale (nonaxisymmetric) oscillations at times $t>1.8$, as shown in the image of Fig. 6, which ultimately cause transient turbulence. In addition, a second instability can be seen at later times at the outer region B (a short wavelength mode that is modulated on a longer length scale around the torus). Our axisymmetric computations are, of course, unable to capture these three-dimensional wavelike structures and so we note an understandable divergence between experiment and computation in Fig. 5 at times beyond $t\approx1.5$. The small-scale wavelike instability appears to be entirely a consequence of the front development.

In summary, at leading order for large Re, the (local)

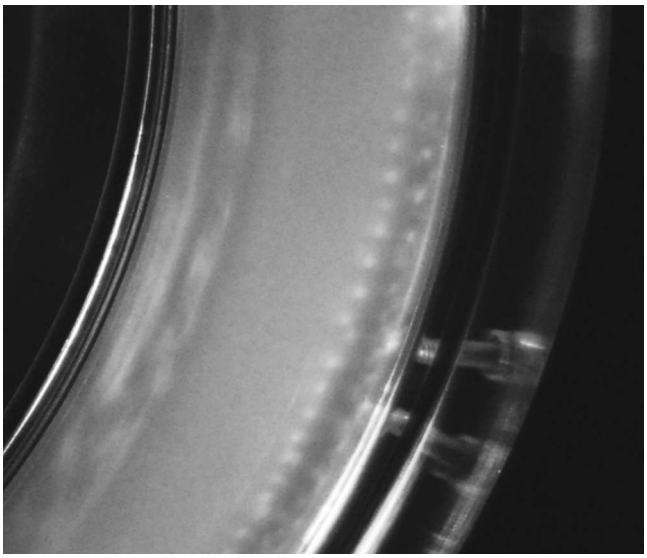

FIG. 6. At times greater than $t \approx 1.8$, when Re=3960, a nonaxisymmetric wave instability can be observed at both equatorial regions.

boundary layer near region *A* evolves to a finite-time singularity, with a thickness that increases without bound. Clearly, on approaching the singularity at large (but finite) Reynolds number, other effects come into play to prevent the singularity from being realized in the full field equations. Our experimental results in Fig. 5 show that the flow remains axisymmetric at this point; therefore a likely candidate for mitigation of the singularity is simply the reintroduction of pressure variations across the boundary layer. Nonetheless, this singularity still has a dramatic physical consequence at large but finite values of Re; it is indicative of a very rapid expansion (unsteady separation) of the viscous layer with a large-scale ejection into the core flow.

V. CONCLUSIONS

The toroidal geometry discussed herein provides an ideal domain, with well defined boundary conditions, that allows us to consider whether (finite-time) singularities of the boundary-layer equations lead to observable (bulk) experimental events and how they connect to detailed numerical solutions at finite (but small) Ekman numbers.

Through careful experimental measurement, we can follow the propagation of a flow front from the inner wall of a rotating fluid-filled torus that is suddenly brought to rest. By analyzing the boundary layer in the vicinity of region *A*, we deduce that at early times this front can be quantitatively connected to an eruption of the viscous layer adjacent to the container wall and to a finite-time singularity in the boundary-layer equations. The singularity is associated with increasingly rapid growth of the boundary-layer thickness. The progress of this ejected fluid matches that of the experimentally observed front, indicating the identity of this flow feature.

There has been much discussion and speculation on the relationship between unsteady separation and flow instabilities. For the unsteady separation induced by a vortex above a plane wall, Brinckman and Walker[7] reported the presence of longitudinal disturbances that have wavelengths that scale with the thickness of the boundary layer, the hallmark of a Rayleigh instability. The results of Ref. 8 show that these features are sensitive to numerical resolution but nonetheless conjecture that they may be physical. Intriguingly, the wavelike instabilities that have been observed in our experiments (in the ϕ direction, a longitudinal coordinate in the torus configuration) are of short wavelength, and we conjecture that they scale with the boundary-layer thickness. Although the spin-down flow in a torus is three-dimensional, it may be a better geometry to study unsteady separation and the role played by small-scale instabilities, allowing numerical, asymptotic, and, crucially, experimental results to be compared.

ACKNOWLEDGMENTS

Work undertaken by R. J. Clarke and J. P. Denier on this study was supported by Australian Research Council Grant No. DP0556360.

[1] H. P. Greenspan and L. N. Howard, "On a time-dependent motion of a rotating fluid," J. Fluid Mech. **17**, 385 (1963).
[2] H. P. Greenspan, *The Theory of Rotating Fluids* (Cambridge University Press, Cambridge, 1968).
[3] F. N. Madden and T. Mullin, "The spin-up from rest of a fluid-filled torus," J. Fluid Mech. **265**, 217 (1994).
[4] W. H. H. Banks and M. B. Zaturska, "The collision of unsteady laminar boundary layers," J. Eng. Math. **13**, 193 (1979).
[5] C. J. Simpson and K. Stewartson, "A note on a boundary-layer collision on a rotating sphere," ZAMP **33**, 370 (1982).
[6] J. H. Siggers and S. L. Waters, "Steady flows in pipes with finite curvature," Phys. Fluids **17**, 077102 (2005).
[7] K. W. Brinckman and J. D. Walker, "Instability in a viscous flow driven by streamwise vortices," J. Fluid Mech. **432**, 127 (2001).
[8] A. V. Obabko and K. W. Cassel, "On the ejection-induced instability in Navier–Stokes solutions of unsteady separation," Philos. Trans. R. Soc. London, Ser. A **363**, 1189 (2005).